Integrating concentrated solar power with storage into a conventional coal-fired power plant for feedwater heating

Murray Starr[1], Michael Owen[2]

[1] Stellenbosch University, Department of Mechanical & Mechatronic Engineering, Private Bag X1 Matieland 7602

Stellenbosch, South Africa; Phone: +27826184414; E-mail: murray@starr.co.za

[2] Stellenbosch University; E-mail: mikeowen@sun.ac.za

Abstract: Solar Aided Power Generation is considered for the South African context by using solar thermal energy for feedwater heating in a 500 MW_e coal-fired power plant under standard operating conditions. A central receiver concentrated solar power (CSP) system is considered for the solar component. In addition, thermal energy storage (TES) is incorporated due to its ability to increase the capacity factor of the plant and provide flexible / constant thermal energy input to the coal cycle. The study predicts a minimum LCOE of 0.09315 USD/kWh of "green" electrical energy for the SAPG plant with a Solar Multiple (SM) of 3.93 and 9 hours of TES. The LCOE of the SAPG plant is 0.0358 USD/kWh lower than that of a stand-alone CSP central receiver power plant using the same costing parameters. The SAPG plant, operating in power boost mode, is predicted to produce an additional 256.17 GWh/annum of electrical energy relative to the stand-alone coal-fired power plant (5.68%). This amounts to a potential emission offset of 183.9 kT CO_2-eq per annum.

Keywords: Solar aided power generation; Coal-fired power plant; Hybridization; Concentrated solar power; Renewable energy; Thermal energy storage.

1. Introduction

Coal-fired power stations currently contribute approximately 76% of South Africa's total electricity generation [1]. With the largest coal-fired power plant in South Africa currently under construction, coal continues to provide South Africa with a cheap and reliable energy source. Since fossil fuels will remain a prominent means of electricity generation, methods to capitalize on existing infrastructure while simultaneously reducing the environmental impact of producing electricity are warranted. The topic of hybrid renewable energy/fossil fuel energy generation is explored in this study by analysing the integration of solar thermal energy into a conventional coal-fired power plant to offset coal consumption and / or provide renewable energy generation.

By making use of the hybrid format for power generation, benefits such as infrastructure sharing and the availability of skilled personnel on site lower the implementation costs of the renewable energy [2]. Power supply can thus be achieved with the benefit of reducing overall coal consumption and related emissions and generally moving towards a future with less dependence on fossil fuels.

With some of the world's highest Direct Normal Irradiation (DNI) values (up to 3200 W/m^2 [3]), South Africa is well suited to solar thermal energy technologies such as concentrating solar power (CSP). The main advantages of CSP are its ability to integrate thermal energy storage (TES) and its scalability such that it can be used to provide thermal outputs similar to that of conventional fossil fuel generation [4].

This study will investigate a solar-aided power generation scenario consisting of a central receiver CSP plant with molten salt TES providing feedwater heat to a generic 500 MW_e coal-fired Rankine cycle. The analysis is conducted using annual insolation data for a location in South Africa's coal rich province of Mpumalanga, where many coal-fired power plants are located, and presents a relatively high level feasibility analysis of the SAPG plant based on LCOE, annual energy production and the possible emission reductions associated with the system. A stand-alone CSP plant is also considered for comparative purposes.

2. Solar Aided Power Generation

SAPG was first researched in 1975 by Zoschak and Wu [5] who investigated seven different methods for integrating solar thermal energy, from a central receiver CSP plant, into an 800 MW_e coal-fired power plant. The methods of heat

integration studied were feedwater heating, superheating of steam, evaporation of water, combined evaporation and superheating, air preheating, reheating of steam and combined air preheating. Results demonstrated that feedwater heating was a desirable option in terms of technical design, capital costs and operating aspects. In such a scenario, solar heat is used to offset feedwater heating bleed steam in a regenerative Rankine cycle resulting in increased mass flow rate through the steam turbine(s) and therefore increased power generation.

The SAPG concept has important thermodynamic advantages over conventional stand-alone solar thermal power generation systems [6,7] since the maximum cycle heat source temperature is not limited by the solar thermal energy input but rather the fossil fuel combustion temperature, which greatly exceeds the solar input temperature, benefitting the solar to power efficiency of the SAPG [8,9]. Further possible SAPG advantages, identified by Hu *et al.* [2], are summarized below:

- Higher thermodynamic energy efficiencies compared to normal coal-fired and stand-alone solar plants.
- A relatively low implementation cost coupled with environmental, social and economic benefits as a result of utilizing existing resources such as grid connection and skilled personnel on site.
- SAPG technology can be applied to new plants or as a retrofit to existing plants with low risk.
- The integration techniques for a SAPG plant are flexible. Depending on the capital available, the solar addition can be implemented in stages.
- SAPG plants can be operated in two ways, either increasing the coal plant's power output whilst keeping the fuel consumption constant - referred to as power-boosting (PB) mode, or by reducing fuel consumption and keeping the power output constant - fuel-saving (FS) mode.

Li *et al.* [10] studied the performance of a 600 MW_e coal-fired SAPG power plant with TES under different loads (100 %, 75 % and 50 %) with different solar shares using CSP central receiver technology. Simulations were conducted with the summer or winter solstice solar irradiance figures from a location in China where DNI annual totals are 2 539 kWh/m^2. The study included the effects of solar multiple (SM) and TES size on the daily performance of SAPG system operating in FS mode. The study proved that fuel savings are functions of SM and TES size and found that during periods of high solar irradiation, the coal consumption was the lowest for SM = 2.2 and 8 hours of TES. In the South African context, PB mode is likely to be more relevant as a result of our national electricity generation shortfall.

3. SAPG plant modelling

A SAPG system (see Fig. 1), including a central receiver CSP plant with molten salt TES and the primary coal-fired steam cycle was modelled in MATLAB (version R2018b). An annual simulation was conducted consisting of quasi-steady-state hourly calculations dependent on hourly Typical Meteorological Year (TMY) weather conditions generated by Meteonorm V.7.3.1, using a location in Mpumalanga, South Africa (26.26° S, 29.26° E). The schematic diagram of the reference coal power plant is shown in Fig. 1 (a). The design parameters of the reference power plant were taken from a study conducted by Rashidi et al. [11]. The key SAPG plant parameters are detailed in Table 1.

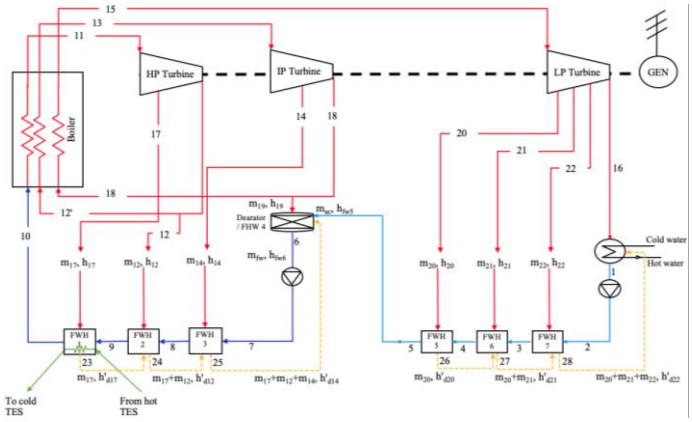

(a)

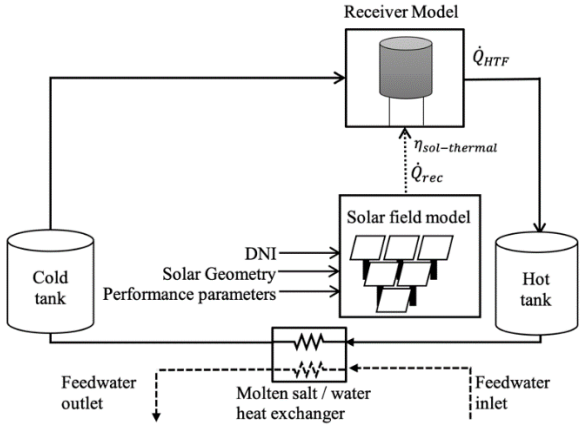

(b)

Fig. 1. Schematic diagram of the SAPG plant (a) 500 MWe Rankine cycle [11], (b) CSP component

3.1. CSP component

The CSP component (Fig. 1 (b)) consists of a heliostat field, central receiver tower, heat exchanger and hot and cold TES tanks. The performance of the system is a function of the solar resource which is characterized by the solar geometry and time. The following sub-sections describe the components of the CSP

model.

Table 1. Main design parameters of the SAPG plant

Systems	Parameters	Value	Unit
CSP power plant	Annual DNI	2177.85	kWh/m^2
	Single heliostat area	2.23	m^2
	Solar field area range	167640.62 – 838203.09	m^2
	SM range	1 – 6	-
	TES range	0 – 16	Hours
	Rated thermal energy transferred to coal-fired power plant at FWH-1	91.889	MW_{th}
Coal-fired power plant	Generating capacity	506.37	MW_e
	Parameters of feedwater inlet to boiler (point 10 in Fig. 1)	30 / 340.8 / 1551	MPa / °C / kJ·kg^{-1}
	Parameters of feedwater inlet to boiler (point 11 in Fig. 1)	30 / 600 / 3443	MPa / °C / kJ·kg^{-1}
	Cold water	25	°C
	Hot water	35	°C

3.1.1.Solar geometry and solar time

The vector approach prescribed by Stine and Geyer [12] was used to determine the sun's position, characterized by the transient azimuth (γ_s) and zenith (θ_Z) angles, relative to the CSP plant. The site's geographical data (longitude and latitude) is used to calculate the solar time, t_s from the local clock time (*LCT*) in 24-hour format using Equation 1.

$$t_s = \frac{EOT}{60} - LC + LCT \quad (1)$$

where, LC is the longitudinal correction based on the difference between the longitude of the plant (φ_{local}) and the standard time zone meridian (φ_{stm}) as shown in Equation (2), and EOT is the equation of time (in minutes) presented in Equation (3).

$$LC = \frac{(\varphi_{local}) - (\varphi_{stm})}{15} \quad (2)$$

$$EOT = 0.258\cos x - 7.416\sin x - 3.648\cos(2x) - 9.228\sin(2x) \quad (3)$$

where, x represents the day of the year in angular value determined using Equation (4).

$$x = \frac{360(N-1)}{365.242} \quad (4)$$

with N being the specific day under consideration (i.e. 1st January = 1; 31st December = 365).

The solar time (t_s) is used to calculate the hour angle (ω), using Equation (5), which indicates the sun's position with respect to the local meridian.

$$\omega = 15(t_s - 12) \quad (5)$$

The declination angle (between the sun's position and the earth's equatorial plane) (δ) is calculated with Equation (6).

$$\sin\delta = 0.39795\cos\big(0.98563(N-173)\big) \quad (6)$$

Equations (1) to (6) are used to calculate the zenith angle, θ_Z as follows:

$$\theta_Z = \cos^{-1}[\cos\phi\cos\delta\cos\omega + \sin\phi\sin\delta] \quad (7)$$

where ϕ is the latitude coordinate of the site.

The azimuth angle (γ_s) is measured clockwise on the horizontal plane, from the north-pointing coordinate axis to the projection of the sun's central ray and is calculated using Equation (8) [13].

$$\gamma_s = \sin(\omega)\left|\cos^{-1}\left(\frac{\cos\theta_z\sin\emptyset - \sin\delta}{\sin\theta_z\cos\emptyset}\right)\right| \quad (8)$$

The azimuth and zenith angles are sent to the heliostat component to model the optical performance of the solar field for each time step.

3.1.2.Heliostat field

The heliostat field reflects the incident solar radiation towards a centrally located receiver tower. The radiative power reflected onto the receiver by the heliostat field is calculated using Equation (9) [14].

$$\dot{Q}_{rec} = A_{SF}\cdot DNI\cdot\eta_{opt,field}\cdot\eta_{opt,0} \quad (9)$$

where, A_{SF} is the total reflective area of the heliostat field, $\eta_{opt,0}$ is the fixed optical efficiency of the heliostat field and $\eta_{opt,field}$ is the instantaneous optical efficiency of the heliostat field which is dependent on zenith angle (θ_Z) and accounts for shading, blocking and cosine effects.

Equation (10) [15] was used to determine the instantaneous optical efficiency of the entire heliostat field.

$$\eta_{opt,field} = 0.4254{\theta_Z}^6 - 1.1480{\theta_Z}^5 + 0.35070{\theta_Z}^4 + 0.755{\theta_Z}^3 - 0.5918{\theta_Z}^2 + 0.0816\theta_Z + 0.832 \quad (10)$$

The fixed optical efficiency of the heliostat field is determined by the performance parameters of the individual heliostats using Equation (11).

$$\eta_{opt,0} = c_f\,\eta_{atten}\eta_{refl}\eta_{spill} \quad (11)$$

These performance parameters include the cleanliness (c_f) and the reflectivity (η_{refl}) of the mirror surface, atmospheric

attenuation (η_{atten}) and spillage (η_{spill}). The values / expressions used for these parameters are given in Table 2.

Table 2: Heliostat performance parameters

Parameter	Value	Reference
c_f	0.95	[14]
η_{refl}	0.95	[14]
η_{atten}	Equation (12)	[16]
η_{spill}	0.90	[16, 17]

$$\eta_{atten} = 0.99321 - 0.001176r + 1.97 \times 10^{-8} r^2 \quad (12)$$

3.1.3.Receiver

Solar radiation reflected by the heliostat field is focused onto the receiver and the temperature of the molten salt heat transfer fluid (HTF) increases by absorbing heat from the receiver as per Equation (13).

$$\dot{Q}_{HTF} = \dot{Q}_{rec} \cdot \eta_{sol-thermal} \quad (13)$$

A solar-to-thermal efficiency of the receiver ($\eta_{sol-thermal}$) of 80 % [16] was assumed to account for convective and radiative losses associated with external type receivers.

3.1.4.Molten salt / water heat exchanger

The link between the energy storage models, the receiver model and the heliostat field are illustrated in Fig. 1(b).

The temperature of the HTF entering the hot tank is assumed to be the temperature of the HTF leaving the receiver. Similarly, the temperature of the HTF leaving the cold tank is assumed to be the temperature entering the receiver.

The model in this study makes use of the constant temperature approach, whereby the mass flow rate of the HTF is adjusted accordingly to maintain a constant HTF temperature exiting the receiver as well as exiting the molten salt / water heat exchanger. The mass flow rate of the HTF adapts according to the available solar thermal energy at the receiver ($\dot{Q}_{rec}$). The exit temperature of the HTF exiting the hot tank and flowing into the molten salt / water heat exchanger is 575°C. Similarly to the receiver, the mass flow rate of the HTF through the molten salt / water heat exchanger is adjusted accordingly to ensure the exit temperature of the HTF does not drop below the exit temperature of the feedwater exiting the FWH under study, this being 340°C. This is done to ensure heat from the HTF is only transferred to the feedwater stream.

3.1.5.TES

The TES system modelled is an active direct system using molten salt as the storage medium. The TES system was modelled as being 98.5% efficient (η_{TES}) [19]. As more heat is transferred to the HTF through the receiver, the HTF is either directed to the TES tank, during times of high irradiation, or directed to the molten salt / water heat exchanger to heat the feedwater. TES is sized according to the number of hours of operation the TES can supply heat at the rated feedwater heater which is to be replaced using Equation (14).

$$\dot{Q}_{TES\,max} = Hours * \dot{Q}_{FWH-1} \quad (14)$$

3.1.6.Sizing of the solar field

The reflective area of the solar field (A_{SF}) was chosen to meet the full heat load supplied by bleed steam to FWH-1 ($\dot{Q}_{FWH-1}$) at the maximum DNI experienced in the TMY as shown in Equation (15).

$$A_{SF} = SM\left(\frac{\dot{Q}_{FWH-1}}{\eta_{opt,field} \cdot \eta_{opt,0} \cdot \eta_{sol-thermal} \cdot \max(DNI)}\right) \quad (15)$$

In this study $\dot{Q}_{FWH-1}$= 91 889.59 kW_{th} [11] and $0.167 \leq A_{SF} \leq 0.838$ km^2.

3.2. Primary coal-fired steam cycle

A 500 MW_e bituminous coal-fired Rankine cycle with double reheat and regeneration was used as the reference power plant. Only full load operation was considered. It is however noted that coal-fired power plants rarely operate at 100 % load throughout the year due to the large variation in annual electricity demand [20]. To accurately predict the effect of the CSP integration, each component was assessed sequentially in the path of the steam flow. Since this paper aims to offer a relatively high level feasibility analysis, the cycle components were modelled based on the simplifying assumptions discussed in the following subsections. All numbers below refer to positions in Fig. 1(a).

3.2.1.Boiler

The boiler is treated as a constant heat transfer rate component with three steam stream inputs: the feedwater steam (10), the first reheat (12') and second (18) reheat streams. The thermal heat input rate in the boiler is calculated based on design conditions using Equation (16).

$$\dot{Q}_{in,total} = \sum \dot{Q}_{in,i} = \dot{m}_{10}(h_{11} - h_{10}) + \dot{m}_{12'}(h_{13} - h_{12'}) + \dot{m}_{18}(h_{15} - h_{18}) \quad (16)$$

where, h is the specific enthalpy of a respective stream through the boiler and $\dot{m}$ is the mass flow rate of the water through each stream; Using the information presented in [11], $\dot{Q}_{in,total} = 1\,002.91\ MW_{th}$.

In the SAPG system bleed steam from the HP turbine (17) is replaced by solar heat meaning that more steam flows through the HP turbine and to the first and second reheat loops. By assuming constant heat supply in the boiler, the enthalpy at the boiler outlet in each stream was calculated using Equation (17).

$$h_{out}{}' = \frac{\dot{Q}_{in,i}}{\dot{m}_{Boiler\ stream}} + h_{in}$$

$$(i = 12' - 13, 18 - 15) \quad (17)$$

3.2.2.Feedwater heaters

The SAPG plant was controlled to ensure the condition of the feedwater to the inlet of the boiler (10) was kept constant throughout the simulation by adjusting the supply of bleed steam to FWH 1 ($\dot{m}_{17}$) depending on the supply of solar heat.

All FWHs except the deaerator (FWH 4) are typical closed-FWHs. In conventional steam cycles, feedwater heating efficiency is increased by making use of the cascade flow of upstream FWHs drain water. The cascade flow can be seen in Fig. 1 with the yellow dashed line. The model adopted for each FWH is given in Equation (18).

$$\dot{m}_{fw,i}\Delta h_{fw,i} = \dot{m}_i\Delta h_{bs,i} + \dot{m}_d\Delta h_{dw,i} \quad (18)$$

where, $\Delta h_{dw,i}$ is the specific drop in drain water enthalpy (Equation(19)); $\dot{m}_{fw,i}$ is the feedwater mass flow rate; $\Delta h_{fw,i}$ is the specific increase in feedwater enthalpy (Equation (20)); $\dot{m}_i$ is the bleed-steam mass flow rate; $\Delta h_{bs,i}$ is the specific drop in enthalpy of the extracted bleed steam (Equation (21)); $\dot{m}_d$ is the cascade drain water mass flow rate.

$$\Delta h_{dw,i} = \begin{cases} h_{d,i-1} - h_{d,i}\ (i = 2,3,5,6,7) \\ h_{d,3} - h_{fw,5}\ (i = 4) \end{cases} \quad (19)$$

$$\Delta h_{fw,i} = h_{fw,i} - h_{fw,i+1} \quad (20)$$

$$\Delta h_{bs,i} = \begin{cases} h_i - h_{d,i}\ (i = 1,2,3,5,6,7) \\ h_i - h_{fw,5}\ (i = 4) \end{cases} \quad (21)$$

where h_i is the specific enthalpy of the bleed-steam entering the i_{th} FWH; $h_{d,i}$ is the specific enthalpy of the drain water from the i_{th} FWH; $h_{fw,i}$ is the specific enthalpy of the feedwater at the FHW inlet.

3.2.3.Steam turbines

The steam turbines were modelled as constant efficiency and pressure drop components with values for these metrics extracted from [11] and given in Table 3.

Table 3: Steam turbine efficiencies and pressure drops

Turbine	Δ Pressure, P [kPa]	Density, ρ [kg/m^3]	Efficiency, η [%]
HPT (11-17)	14 879.00	68.85	85.1
HPT (17-12)	6 814.00	40.52	83.3
IPT (13-14)	5 030.00	15.79	92.3
IPT (14-18)	2 078.00	7.31	90.1
LPT (15-20)	871.30	2.02	94.9
LPT (20-21)	186.10	0.79	88.5
LPT (21-22)	76.60	0.41	85.0
LPT (22-16)	55.00	0.17	90.1

The turbine power ($\dot{W}$) output was as shown in Equation (22).

$$\dot{W} = \dot{m}\,(h_{inlet} - h_{exit}) = \frac{\Delta P\eta}{\rho}\dot{m} \quad (22)$$

where ρ is the average density of the inlet steam flow and outlet steam flow.

The introduction of the solar thermal heat input inevitably leads to the changes of steam flow rate in various flow paths as well as thermal parameters in the turbine. Using Equation (17) and (22), each stage of the turbine work output could be determined depending on the properties and flow rate of steam entering and exiting each turbine stage.

3.2.4.Condenser

The exhaust steam from the final LPT stage is condensed to water for re-use in the boiler (feedwater). Constant temperature across the condenser was assumed in the condenser model. Therefore, the condensing pressure at the exit of the condenser remains constant throughout the simulation.

3.3. Emission reduction

The annual emissions offset, quantified in tons of CO_2 equivalent, due to the additional clean energy produced as a result of the replacement of bleed steam in a conventional coal-fired power plant with solar heat was estimated using Equation (23).

$$CO_2eq\ offset = CFPP\ emission\ factor \times E_{SAPG\ increase,a} \quad (23)$$

where $E_{SAPG\ increase,a}$ represents the annual electrical energy increase in the SAPG plant due to the CSP integration. The amount of CO_2-eq. offset on an annual basis depends on the coal-fired power plant emission factor which is estimated to be 718 g CO_2-eq/kWh [21].

3.4. Stand-alone CSP Plant

The power output from a stand-alone CSP plant (P_{eq}) with its

own power block is approximated by making use of the modified Carnot efficiency [22] and the solar thermal heat input ($\dot{Q}_{HTF}$) ut as shown in Equation (24). The power block is sized based on $\dot{Q}_{FWH-1}$ as per Section 3.1.6.

$$P_{eq} = \dot{Q}_{HTF} \times \left(1 - \sqrt{\frac{T_C}{T_H}}\right) \quad (24)$$

where T_C and T_H are the respective temperatures (in K) of the heat sink (Cold water in Fig. 1) and heat source (Molten Salt temperature: 575°C).

4. Financial model

Equation (25) [23] was used to calculate the LCOE of the increased electricity produced by the SAPG plant.

$$LCOE = \frac{CRF \times CAPEX + OPEX}{W_{SAPG\ increase,a}} \quad (25)$$

where CRF is the capital recovery factor defined in Equation (26); $CAPEX$ is the capital expense, taking into account both the direct and indirect costs of constructing the CSP plant; and $OPEX$ is the annual CSP operational and maintenance costs.

$$CRF = \frac{k_d(1+k_d)^n}{(1+k_d)^n - 1} \quad (26)$$

where k_d is the is the annual discount rate, and n is expected project lifetime.

A discount rate of 8 % and a project lifetime of 20 years were used in the analysis. 20 years was considered for the expected project lifetime as this is the typical length of a Power Purchasing Agreement (PPA) within the South African REIPPPP. Capital and operating expense parameters as well as the discount rate was selected based on the study conducted by Poole [14] shown in Table 4 and Table 5.

Table 4. Capital expense parameters [14]

Capital expense description	Cost	Unit
Land cost	0.2	USD/m^2
Site improvements	16.0	USD/m^2
Heliostat field	170.0	USD/m^2
Receiver and tower	173.0	USD/kW$_{th}$
Thermal energy storage	26.0	USD/kW$_{th}$
Steam turbine system	900.0	USD/kW$_e$
Steam generating system	300.0	USD/kW$_e$

Table 5: Annual operating expense parameters [24]

Operating expense description	Cost	Unit
Fixed cost by capacity	72.0	USD/kW$_e$-year
Variable cost	4.0	USD/MWh$_e$

5. Results

5.1. LCOE

LCOE of the additional energy from the SAPG plant was investigated with TES size ranging between 0 and 16 hours and for 1 ≤ SM ≤ 6 with results shown in Fig. 2.

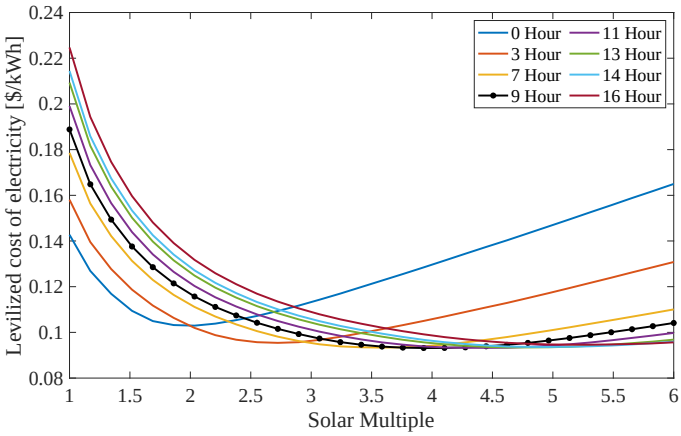

Fig. 2. LCOE variation with SM and TES hours

TES becomes financially attractive for SM > 2 and always results in lower LCOE than without TES for SM > 2.8. An absolute minimum LCOE of 0.09316 USD/kWh (~1.33 ZAR/kWh) is realised with 9 hours of TES and a SM of 3.93.

In comparison Adibhatla and Kaushik's [25] report LCOE = 0.0640 USD/kWh for SAPG using a CSP parabolic trough system with 7 hours of TES and a SM of 4 for feedwater heating at the final FWH in a 500 MW$_e$ coal-fired power plant. The difference in LCOE and optimal configuration may be attributed to the different CSP technology and Adibhatla and Kaushik's consideration of FS mode, a 25 year project life and cost estimates from 2012.

5.2. Annual power generation

The annual electrical power generation of the SAPG plant was compared to the conventional 500 MW$_e$ coal-fired power plant (no SAPG) and a stand-alone CSP plant, using the lowest LCOE design found in section 5.1 (9 hour of TES and SM of 3.93). Fig. 3 shows the power boosting potential of the SAPG plant. A 5.68 % (256.16 GWh) annual increase in electrical energy production is predicted through the incorporation of SAPG.

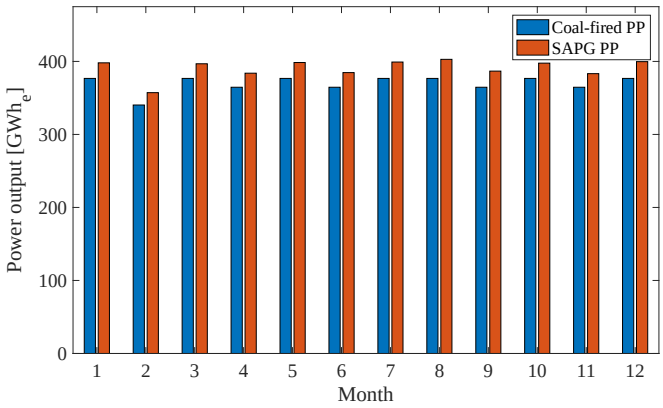

Fig. 3. Comparison of electricity generated for conventional coal-fired power plant and SAPG plant

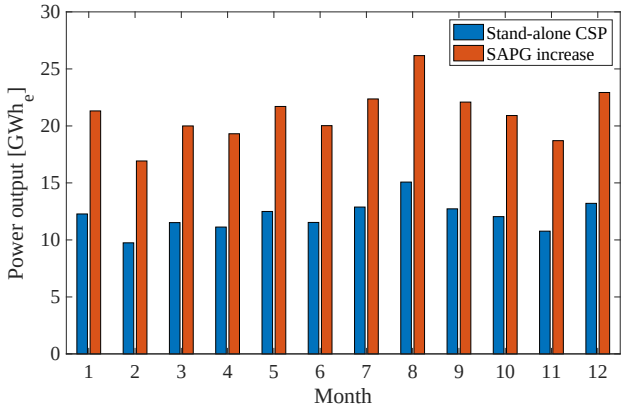

Fig. 4. Comparison of electricity generated for stand-alone central receiver power plant and an SAPG plant increase

The monthly electrical energy output of a stand-alone CSP central receiver power plant and the increase in electrical energy output of the SAPG plant is shown in Fig. 3.

The SAPG plant outperforms a stand-alone CSP central receiver power plant by producing 1.7 times the annual energy with the same solar field size. Pierce [26] found that an SAPG plant, used for preheating of feedwater, used the available solar thermal energy 1.5 times more effectively than that of a stand-alone CSP parabolic trough plant. Pierce's [26] findings however did not include TES. Taking into account the increase in capacity factor due the inclusion of TES, the findings of this study are feasible.

5.3. Annual emissions reduction

As the plant is run in PB mode the increase in electrical energy output of the SAPG plant compared to that of the coal-fired power plant is realised at the same rate of coal consumption. The SAPG-related increase in electrical energy output is therefore "emissions free". Fig. 5 presents the amount of CO_2-eq. emissions that would have been generated had the additional energy been produced by burning more coal (i.e. the emissions offset) as a function of SM and TES size. An offset of 183.9 kT CO_2-eq. is predicted for the lowest LCOE case identified in section 5.1. Greater emissions offsets can obviously be realised with greater SM and TES size but at greater cost.

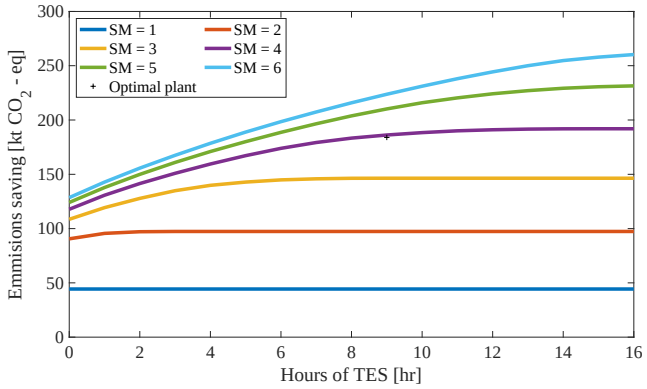

Fig. 5. SAPG related CO_2-eq offset

6. Conclusions

This paper considers power boosting SAPG in a specific 500 MW_e coal-fired power plant (double reheat and regeneration) in a representative location in South Africa. The solar component consisted of a central receiver CSP system with molten salt TES. The solar heat was used for feedwater heating and replaced bleed steam in the final FWH. A stand-alone central receiver CSP plant was also modelled for comparative purposes.

A solar field with SM = 3.93 (~0.66 km^2) and 9 hours of TES was predicted to offer the most financially attractive solution with LCOE = 0.09315 USD/kWh (1.33 ZAR/kWh). According to Poole [14], LCOE = 0.12895 USD/kWh (1.84 ZAR/kWh) for a stand-alone central receiver CSP power plant in South Africa. The SAPG plant therefore offers a 28% reduction in the LCOE of solar generated electricity. With SM = 3.93 and 9 hours of TES, an annual SAPG related energy increase 256.17 GWh (or 5.68 % of the annual coal-plant output at full load) was predicted with an associated 183.9 kT CO_2-eq. emissions offset. The annual SAPG related energy production also exceeded the stand-alone CSP plant product by 70%.

This study is subject to constraints of certain assumptions, particularly within the coal-fired power plant. The model used in

this study was developed for full-load operation whereas part load behaviour is witnessed in most conventional coal-fired power plants. Nonetheless, from a financial and technical viewpoint, the proposed SAPG plant with TES is shown to be feasible. The model used in this study predicts favourable technical and financial characteristics compared to similar stand-alone CSP projects within South Africa and the global context.

References

[1] Department of Energy, "Integrated Resource Plan (IRP2019)," Pretoria, 2019.

[2] E. Hu, Y. Yang, A. Nishimura, F. Yilmaz, and A. Kouzani, "Solar thermal aided power generation," *Appl. Energy*, vol. 87, no. 9, pp. 2881–2885, Apr. 2010, doi: 10.1016/j.apenergy.2009.10.025.

[3] The World Bank, "Solar resource maps of South Africa," *Solar resource maps of South Africa*, Apr. 23, 2017. https://solargis.com/maps-and-gis-data/download/south-africa/.

[4] P. Naicker and G. A. Thopil, "A framework for sustainable utility scale renewable energy selection in South Africa," *J. Clean. Prod.*, vol. 224, pp. 637–650, 2019, doi: 10.1016/j.jclepro.2019.03.257.

[5] R. J. Zoschak and S. F. Wu, "Studies of the direct input of solar energy to a fossil-fueled central station steam power plant," *Sol. Energy*, vol. 17, no. 5, pp. 297–305, 1975, doi: 10.1016/0038-092X(75)90047-X.

[6] J. Qin, E. Hu, and X. Li, "Solar aided power generation: A review," *Energy Built Environ.*, vol. 1, no. 1, pp. 11–26, Sep. 2020, doi: 10.1016/j.enbenv.2019.09.003.

[7] W. Pierce, P. Gauché, T. Von Backström, A. C. Brent, and A. Tadros, "A comparison of solar aided power generation (SAPG) and stand-alone concentrating solar power (CSP): A South African case study," *Appl. Therm. Eng.*, vol. 61, no. 2, pp. 657–662, 2013, doi: 10.1016/j.applthermaleng.2013.08.014.

[8] E. Hu, Y. Yang, and A. Nishimur, "Solar Aided Power Generation: Generating 'Green' Power from Conventional Fossil Fuelled Power Stations," in *Thermal Power Plants*, InTech, 2012, p. 18.

[9] Y. Yang, Q. Yan, R. Zhai, A. Kouzani, and E. Hu, "An efficient way to use medium-or-low temperature solar heat for power generation - Integration into conventional power plant," *Appl. Therm. Eng.*, vol. 31, no. 2–3, pp. 157–162, 2011, doi: 10.1016/j.applthermaleng.2010.08.024.

[10] C. Li, Z. Yang, R. Zhai, Y. Yang, K. Patchigolla, and J. E. Oakey, "Off-design thermodynamic performances of a solar tower aided coal-fired power plant for different solar multiples with thermal energy storage," *Energy*, vol. 163, pp. 956–968, 2018, doi: 10.1016/j.energy.2018.08.186.

[11] M. M. Rashidi, A. Aghagoli, and M. Ali, "Thermodynamic analysis of a steam power plant with double reheat and feed water heaters," *Adv. Mech. Eng.*, vol. 2014, no. March, 2014, doi: 10.1155/2014/940818.

[12] W. Stine and M. Geyer, *Power From The Sun*. 2001.

[13] J. Duffie and W. Beckman, *Solar Engineering of Thermal Processes, 4th Edition*. 2013.

[14] I. V. Poole, "Concentrating solar power in South Africa - a comparison between parabolic trough and power tower technologies with molten salt as heat transfer fluid," Stellenbosch University, 2017.

[15] P. Gauché, S. Pfenninger, and A. J. Meyer, "Modeling dispatchability potential of CSP in South Africa," in *South African Solar Energy Confrence (SASEC)*, Jun. 2012, p. 11.

[16] F. Biggs and C. N. Vittitoe, "Helios model for the optical behavior of reflecting solar concentrators," New Mexico, 1979. doi: 10.2172/6273705.

[17] F. Rinaldi, M. Binotti, A. Giostri, and G. Manzolini, "Comparison of linear and point focus collectors in solar power plants," *Energy Procedia*, vol. 49, pp. 1491–1500, 2014, doi: 10.1016/j.egypro.2014.03.158.

[18] G. Augsburger, "Thermo-economic optimisation of large solar tower power plants PAR," Federal Institute Of Technology In Lausanne, 2013.

[19] K. Madaly, "Identifying the optimum storage capacity for a 100-MWe concentrating solar power plant in South Africa," Stellenbosch University, 2014.

[20] Y. Zhu, R. Zhai, Y. Yang, and M. Angel Reyes-Belmonte, "Techno-economic analysis of solar tower aided coal-fired power generation system," *Energies*, vol. 10, no. 9, pp. 1–26, 2017, doi: 10.3390/en10091392.

[21] O. Achkari and A. El Fadar, "Latest developments on TES and CSP technologies – Energy and environmental issues, applications and research trends," *Appl. Therm. Eng.*, vol. 167, 2020, doi: 10.1016/j.applthermaleng.2019.114806.

[22] B. Ahlborn and F. L. Curzon, "Efficiency of a Carnot engine at maximum power output," *Am. J. Phys.*, vol. 43, no. 1, pp. 22–24, 1975, doi: 10.1119/1.10023.

[23] W. Short, D. Packey, and T. Holt, "A manual for the economic evaluation of energy efficiency and renewable energy technologies," *Renew. Energy*, vol. 95, no. March, pp. 73–81, 1995, doi: NREL/TP-462-5173.

[24] P. Kurup and C. S. Turchi, "Parabolic Trough Collector Cost Update for the System Advisor Model (SAM)," *Tech. Rep. NREL/TP-6A20-65228 Natl. Renew. Energy Lab.*, no. November, pp. 1–40, 2015.

[25] S. Adibhatla and S. C. Kaushik, "Energy, exergy, economic and environmental (4E) analyses of a conceptual solar aided coal fired 500 MWe thermal power plant with thermal energy storage option," *Sustain. Energy Technol. Assessments*, vol. 21, pp. 89–99, Apr. 2017, doi: 10.1016/j.seta.2017.05.002.

[26] W. T. Pierce, "Solar Assisted Power Generation (SAPG): Investigation of Solar Preheating of Feedwater," Stellenbosch University, 2013.